RESEARCH ARTICLE

A fast target-search framework inspired by micromouse competition and its application in corn disease inspection robots

Chaokun Zhu*

School of Innovation and Entrepreneurship, Kaifeng Vocational College, Kaifeng, Henan, China.

Received: May 18, 2026; **accepted:** September 23, 2026.

Timely inspection of corn diseases is a critical measure to guarantee grain yield. Conventional manual inspection suffers from low efficiency and high missed detection rate, while existing robotic inspection systems have drawbacks including redundant path planning, delayed target recognition, and insufficient adaptability to complex field environments. This study developed an efficient and robust fast target-search framework for corn disease inspection robots to address the bottlenecks of low inspection efficiency and poor environmental adaptability in large-scale corn field scenarios. Inspired by the core mechanisms of fast path exploration, real-time environment perception, and dynamic decision-making in micromouse competitions, this study proposed a micromouse-inspired fast target search framework with a four-level topology of perception, decision, execution, and evaluation layers. The framework integrated four core units including an improved A* path planning module optimized with wall-distance perception and fast turning logic, an integrated detection-segmentation-grading module based on YOLOv8 and U-Net++, a multi-sensor fusion environment perception module combining vision, infrared, Global Positioning System (GPS), and Inertial Measurement Unit (IMU) data, and a disease severity grading module. The results on six corn diseases including large spot disease, small spot disease, and rust showed that the framework achieved a target search success rate of 96.8%, reduced path planning time by 37.2% compared with the traditional A* algorithm, reached a disease segmentation Intersection over Union (IoU) of 0.89, and controlled the missed inspection rate within 3.5%. Under extreme environments such as high temperature, rainy weather, and heavy occlusion, the framework still maintained detection accuracy above 85%, which was significantly superior to existing inspection systems. This study provided an efficient and reliable technical solution for rapid disease inspection in large-scale corn fields and was applicable to the upgrading of modern agricultural intelligent equipment.

Keywords: corn disease; inspection; micromouse competition; fast target search; path planning.

***Corresponding author:** Chaokun Zhu, School of Innovation and Entrepreneurship, Kaifeng Vocational College, Kaifeng, Henan 475100, China. Email: zhuchaokun0511@126.com.

Introduction

As a major grain crop in China, timely inspection of corn diseases is the key to ensuring grain yield. However, traditional manual inspection is inefficient and has a high rate of missed detections, making it difficult to meet the real-time monitoring needs of large-scale agricultural production. Intelligent inspection robots have become the core technology direction to solve this problem.

In recent years, researchers have carried out extensive research on inspection robot

technology, path planning algorithms, and disease detection models. The robot moving target search method proposed by Wong *et al*. provided basic technical support for autonomous inspection systems, but this method did not fully consider the complexity of inter-ridge environments and the specificity of disease targets in agricultural scenarios [1]. The real-time alert investigation method proposed by Liu *et al*. improved the efficiency of threat detection through context-aware priority optimization, but its core focus was on the field of network security and had not been adapted to the accuracy and real-time requirements of agricultural disease detection [2]. Luo *et al*. implemented path planning and computational offloading optimization for multi-UAV collaborative target search based on deep reinforcement learning, achieving breakthroughs in dynamic environment adaptability [3]. However, the adaptability of ground inspection robots in narrow spaces between corn ridges was insufficient. The research on rapid review methods by Garritty *et al*. provided methodological references for sorting out the current status of agricultural intelligent inspection technology and clarified the importance of combining rapid iteration of technology with practical applications [4]. The rapid analysis and reverse design strategy of polymer structures proposed by Liao *et al*. provided an efficient iterative approach for technical optimization, but its cross-domain characteristics made it difficult to directly apply to agricultural robot systems [5]. The research of Merry *et al*. focused on the implementation support factors such as professional competence, intervention compliance, and continuing education, providing practical references for the field promotion of inspection technology, but did not solve the performance bottleneck of the technology itself [6]. Panagoulias *et al*. combined AI interpretability with medical literacy assessment, providing ideas for improving the credibility of disease detection models, but did not involve the overall system integration design of inspection robots [7]. In terms of corn disease inspection research, Okabaka *et al*. designed monitoring robots for corn rust and wilt diseases [8], while Moshayedi *et al*. analyzed the application value of robots in corn planting [9], Stypulkowska proposed an AI judgment robot for corn growth that met the needs of precision agriculture [10], Li *et al*. developed a tactile perception corn leaf phenotype analysis system [11], and Pfordt *et al*. reviewed the application of imaging sensors in corn disease and pest detection [12]. Zhang and Yi studied the motion planning and control strategy of corn inspection robots [13], Diao *et al*. implemented navigation line detection for corn spraying robots based on improved YOLOv10s [14], and Tomas *et al*. used YOLOv7 to achieve image recognition of corn leaf diseases [15]. These studies have promoted the intelligent development of corn disease inspection from different dimensions, but overall, there are still problems such as path planning not adapting to the dynamic changes between ridges, insufficient integration of disease detection-segmentation-grading, lack of environmental adaptive adjustment in multi-sensor fusion, and poor robustness in complex scenes. There are also few studies that draw on the core mechanism of "fast exploration, real-time perception, and dynamic decision-making" in micromouse competitions to optimize inspection efficiency and environmental adaptability.

This research proposed a fast target search framework mimicking micromouse competitions. The study constructed a four-level topology structure, drawing on the closed-loop response mechanism of micromice, adding a disease severity grading module, and achieving collaborative optimization of path planning, target detection, environmental adaptation, and disease assessment. Further, the study proposed an improved A* path planning algorithm that integrated micromouse wall distance perception, steering cost model, and ridge distance adaptive mechanism to balance shortest path, mobility efficiency, and environmental adaptability. Furthermore, this research designed an integrated detection-segmentation-grading module based on the joint improvement of

YOLOv8 and U-Net++, adding a quantitative model for disease severity to enhance the accuracy of disease target recognition, edge segmentation, and grade evaluation. Eventually, the study established a multi-sensor dynamic weighted fusion mechanism, adaptively adjusting the fusion weights of visual, infrared, GPS, and inertial measurement unit (IMU) data based on environmental complexity, and enhancing the robustness of complex environments. The proposed framework provided an efficient target search solution for corn disease inspection robots through hardware platform construction, simulation testing, and field verification, and was suitable for large-scale and complex agricultural intelligent inspection scenarios. The results of this study effectively filled the gaps in existing research on corn disease inspection robots in terms of path planning efficiency, multi-task integration, and complex environment adaptability and provided technical support for the upgrading of intelligent agricultural equipment and the development of precision plant protection.

Materials and methods

Overall design of a fast target search framework for simulating computer mouse competitions

The overall framework adopted a four-level topology structure, drawing on the closed-loop control logic of perception, decision-making and execution in micromouse competitions, and added an evaluation layer to realize disease severity grading. All layers exchanged data and transmitted instructions through Robot Operating System (ROS) nodes, forming a complete closed-loop feedback mechanism. Specifically, the perception layer served as the data input terminal, which acquired multi-source environmental data through Red Green Blue (RGB) cameras, infrared cameras, Global Positioning System (GPS), Inertial Measurement Unit (IMU), ultrasonic sensors, and soil sensors, and transmitted the preprocessed data to the decision layer. The decision layer was the core computing unit of the framework, which consisted of four sub-modules including path planning, disease detection, disease segmentation, and multi-sensor fusion decision-making, and generated inspection instructions according to the input data. The execution layer controlled the mobile chassis, robotic arm, alarm module, and data storage device to complete inspection actions according to the instructions and fed back status information in real time. The evaluation layer classified the severity of diseases based on the identification results and environmental parameters, output prevention and control recommendations, and archived the evaluation results to support subsequent decision optimization.

Path planning module based on improved A * algorithm

Based on the core logic of wall distance perception, path memory and rapid turning in micromouse maze navigation, combined with the variation characteristics of ridge spacing and obstacle distribution in the environment between corn field ridges, this study improved the traditional A* algorithm and constructed a path planning module suitable for operations in corn field ridges [16]. This module consisted of five functional layers from input to output including input layer, preprocessing layer, core calculation layer, optimization layer, and output layer [17]. The input layer received agricultural field geographic information, real-time robot status, historical disease distribution, and environmental dynamic data. The preprocessing layer divided the agricultural field into 10-centimeter square map units, marked each grid as a passable area, an obstacle area or a disease area based on its state, and calculated the distance information between the robot and the ridge as well as the obstacles. The core calculation layer as the key part of the algorithm integrated three sub-modules of heuristic function optimization, path cost calculation, and turning optimization. Based on the traditional A* algorithm, this method introduced turning cost, ridge distance adaptability, and environmental factors for the comprehensive evaluation mechanism of ridge-to-ridge operations,

providing a basis for subsequent path decisions. The improved heuristic function was shown below.

$$h(n)=\omega_1 \cdot d_{euclid}(n, g)+\omega_2 \cdot d_r(n)+\omega_3 \cdot \theta(n)+\omega_4 \cdot C(n) \quad (1)$$

where h(n) was the heuristic function value from node n to target node *g*. ω_1, ω_2, ω_3, and ω_4 were the weight coefficients of Euclidean distance, ridge distance, turning angle, and environmental cost, respectively. $d_{euclid}(n, g)$ was the Euclidean distance between node n and target node *g*, being calculated as $d_{euclid}(n, g)=\sqrt{(x_n-x_g)^2+(y_n-y_g)^2}$; $d_r(n)$ was the distance from node n to the nearest corn ridge, used to ensure that the path traveled along the ridges. When $d_r(n)$ exceeded a reasonable range, a penalty term was added. θ(n) was the turning angle at node n, used to penalize large angle turns and reduce movement time. C(n) was the environmental cost at node n, being calculated based on soil temperature, humidity, and light intensity. The C(n) value increased in low-lying areas prone to flooding or areas with excessive/insufficient light to prevent robots from entering unsuitable work areas [18]. The path cost calculation unit comprehensively considered the path length, movement speed, inspection priority, and remaining power. The total path cost was shown as follows.

$$f(n)=g(n)+h(n) \quad (2)$$

$$g(n)=\alpha \cdot l(n)+\beta \cdot t(n)-\gamma \cdot p(n)+\delta \cdot E(n) \quad (3)$$

where f(n) was the total cost of node n. h(n) was the actual cost from starting point *g(n)* to node n. l(n) was the length of the path from the starting point to node n. t(n) was the travel time of the path. p(n) was the priority for disease inspection in the area where node n was located. E(n) was the cost of remaining power. When the remaining power was below 30%, the E(n) value increased, and priority was given to planning the return path. α, β, γ, and δ were weight coefficients [19]. The steering optimization unit drew on the fast steering logic of computer mice and set a steering angle threshold [20]. When the steering angle of the planned path exceeded the threshold, a segmented steering strategy was adopted to optimize the smoothness of the path by inserting transition nodes, reducing the energy consumption and time consumption of robot steering; Meanwhile, a path memory mechanism was introduced to record the turning characteristics of the traveled path, providing reference for subsequent path planning and avoiding repeated turns. The optimization layer introduced a ridge distance adaptive mechanism, which dynamically adjusted the lateral offset of path planning based on the ridge distance perception value $d_r(n)$ of the preprocessing layer. When the ridge distance changed, the path automatically offset to adapt to the new ridge distance without manual intervention. The output layer converted the optimal path of the core computing layer into executable speed instructions for the robot and stored the inspected path through the path caching unit to avoid repeated inspections, simultaneously output the confidence level T_p of the path planning to evaluate the rationality of the path.

Integrated module of disease target detection segmentation grading

To meet the triple requirements of rapid identification, accurate segmentation, and severity assessment in corn disease inspection, this study constructed a detection-segmentation-grading integrated module based on the joint improvement of YOLOv8 (https://github.com/ultralytics/ultralytics) and U-Net++ (https://github.com/MrGiovanni/UNetPlusPlus). The module adopted the architecture of shared backbone network with three branch heads, which consisted of input layer, feature extraction layer, three task branches and fusion output layer from bottom to top. The input layer received fused images from visual and infrared sensors, performed image enhancement preprocessing to improve robustness, and combined multi-sensor environmental data such as light intensity and temperature. The feature extraction layer used Cross Stage Partial 2f (C2f) modules to preserve fine-grained edge information, Spatial Pyramid

Pooling - Fast (SPPF) modules to fuse multi-scale global features, and Efficient Channel Attention (ECA) (https://github.com/BangguWu/ECANet) modules to adaptively focus on disease areas, together forming an optimized backbone network. The three types of scale feature maps output by it were respectively used for detection, segmentation, and grading, achieving accurate identification and evaluation of diseases of different sizes [21]. The detection branch was based on YOLOv8 detection head improvement, introducing Complete Intersection over Union (CIoU) loss function to optimize bounding box localization, and outputting the bounding box coordinates, category probability P_{class} , and confidence P_{conf} of the disease. The segmentation branch was improved based on U-Net++, and a feature fusion module was added to the decoder part. The bounding box information output by the detection branch was used as a prior to focus on the disease area for accurate segmentation, and output binary segmentation masks and disease area [22]. The grading branch was a newly added module that constructed a disease severity grading model based on the disease area S output by the segmentation branch, the disease category output by the detection branch, and the input environmental data. The grading criteria were as follows.

$$L=\begin{cases}\text{mild} & S<S_1 \ \&\ P_{conf}<0.7 \\ \text{moderate} & S_1\le S<S_2 \ \&\ 0.7\le P_{conf}<0.9 \\ \text{severe} & S\ge S_2 \ \&\ P_{conf}\ge 0.9\end{cases} \quad (4)$$

where L was the severity level of the disease. S_1 and S_2 were area thresholds that were dynamically adjusted according to different types of diseases. P_{conf} was the confidence level of disease detection. An environmental impact factor K was introduced simultaneously. When environmental data indicated high temperature and high humidity, K was set to 1.2, and the severity level was raised by one grade to reflect the environment's role in promoting disease development. To achieve collaborative optimization of detection, segmentation, and grading, a joint loss function was designed as below.

$$L_{total}=\lambda_1\cdot L_{det}+\lambda_2\cdot L_{seg}+\lambda_3\cdot L_{grade} \quad (5)$$

where L_{total} was the total loss function. λ_1, λ_2, and λ_3 were loss weights. L_{det} used a combination of CIoU loss and cross entropy loss for detection loss. L_{seg} was the segmentation loss, which used a combination of Dice loss and Focal loss to solve the problem of pixel imbalance in disease areas. L_{grade} was a classification loss that used cross entropy loss to optimize the accuracy of level classification [23]. The calculations of those factors were shown as follows.

$$L_{seg}=\mu\cdot L_{Dice}+(1-\mu)\cdot L_{Focal} \quad (6)$$

$$L_{Dice}=1-\frac{2\sum_{i=1}^{N} M_i\cdot G_i+\epsilon}{\sum_{i=1}^{N} M_i^2+\sum_{i=1}^{N} G_i^2+\epsilon} \quad (7)$$

$$L_{Focal}=-\sum_{i=1}^{N} G_i\cdot(1-P_i)^{\gamma}\cdot\log(P_i)-\sum_{i=1}^{N}(1-G_i)\cdot P_i^{\gamma}\cdot\log(1-P_i) \quad (8)$$

where G was the true segmentation mask. P_i was the probability of segmentation prediction. μ was the weight coefficient. γ was the focusing parameter of Focal loss. ϵ was a small value used to avoid division by zero. The fusion output layer integrated the category information of the detection branch, the mask and area information of the segmentation branch, and the level information of the classification branch to output the final disease information report [24].

Environmental perception module based on multi-sensor fusion

Drawing on the logic of multi-sensor collaborative perception of maze environment in micromouse competitions and combining with the dynamic change characteristics of complex environments in corn fields, this study constructed a multi-sensor dynamic weighted fusion module suitable for corn field scenarios [25]. The module consisted of six layers including sensor data input layer, data preprocessing layer, dynamic weight calculation layer, fusion decision layer, credibility evaluation layer, and output layer. The input layer gathered real-time data from five categories of sensors including vision, positioning, ultrasound, soil, and illumination.

The preprocessing layer performed targeted filtering and time synchronization on various data and extracted key features of diseases, motion, obstacles, and environment [26]. The dynamic weight calculation layer adaptively assigned fusion weights to each sensor based on environmental complexity, which was quantified by four indicators of light intensity (L), obstacle density (D), terrain slope (S), and temperature and humidity (T/H) as shown below.

$$C=\eta_1 \cdot \frac{L}{L_{max}}+\eta_2 \cdot D+\eta_3 \cdot \frac{S}{S_{max}}+\eta_4 \cdot \frac{T \cdot H}{T_{max} \cdot H_{max}} \quad (9)$$

where C was the complexity of the environment with a value range of 0~1. η_1, η_2, η_3, and η_4 were weight coefficients with values of 0.3, 0.2, 0.2, and 0.3. L_{max} was the maximum illumination intensity. S_{max} was the maximum allowable slope. T_{max} was the maximum allowable temperature. H_{max} was the maximum humidity. Based on the complexity of environment C, the fusion weights of each sensor were dynamically adjusted ω_v as visual sensor weight, ω_g as GPS + IMU weight, ω_u as ultrasound weight, ω_e as environmental sensor weight to satisfy $\omega_v + \omega_g + \omega_u + \omega_e = 1$. When the complexity of the environment was low, the weight of visual sensors was high, relying on visual data to achieve accurate detection. When the complexity of the environment was high, the weight of GPS + IMU and ultrasound was increased, while the weight of environmental sensors remained stable, ensuring the reliability of positioning and obstacle avoidance [27]. The fusion decision layer used the weighted average method to fuse the decision results of each sensor as follows [28].

$$R=\omega_v \cdot R_v+\omega_g \cdot R_g+\omega_u \cdot R_u+\omega_e \cdot R_e \quad (10)$$

where R was the final fusion decision result. R_v was the decision result of the visual sensor. R_g was the decision result of GPS + IMU. R_u was the decision result of the ultrasonic sensor. R_e was the decision result of the environmental sensor. The credibility evaluation layer calculated the credibility T of the fusion result to evaluate the reliability of the fusion result as below.

$$T=\omega_v \cdot T_v+\omega_g \cdot T_g+\omega_u \cdot T_u+\omega_e \cdot T_e \quad (11)$$

where T_v,T_g,T_u,T_e were the self-reliability of each sensor. When $T < 0.6$, the sensor self-test and data acquisition mechanism were triggered to improve fusion reliability. The output layer transmitted the fusion decision results, credibility, and raw data from various sensors to the decision layer, providing data support for path planning and target search [29].

Robot hardware platform

The corn disease inspection robot used in the experiment was equipped with a complete hardware system. The mobile chassis adopted a differential drive structure and was equipped with a 57BL75S10-230TF9 24V DC brushless motor (Dongguan Hengdrive Motor Co., Ltd.; Dongguan, Guangdong, China). The perception system included MV-CA013-21UC RGB camera (Hangzhou Hikvision Digital Technology Co., Ltd., Hangzhou, Zhejiang, China), Vue Pro R infrared camera (FLIR Systems, Inc., Wilsonville, Oregon, USA), NEO-M8N Beidou and GPS dual-mode positioning module (U-blox AG, Thalwil, Switzerland), MPU6050 inertial measurement unit (TDK InvenSense, San Jose, California, USA), 4 units of HC-SR04 ultrasonic sensors (Shenzhen Elecfreaks Technology Co., Ltd., Shenzhen, Guangdong, China), SHT30 temperature and humidity sensor (Sensirion AG, Stäfa, Switzerland), BH1750 illumination sensor (Rohm Semiconductor, Kyoto, Japan), EC-5 soil sensor (Meter Group, Inc., Pullman, Washington, USA). The control core used NVIDIA Jetson Xavier NX embedded development board (NVIDIA Corporation, Santa Clara, California, USA) and STM32F407 microcontroller (STMicroelectronics, Geneva, Switzerland) responsible for visual processing and low-level control, respectively. The robot was powered by 18650 dual-output lithium batteries of 12V and 24V (Shenzhen DMEGC Electronics Co., Ltd., Shenzhen, Guangdong, China), supporting continuous operation for about 8 hours. Inspection data was

stored in real time in a 1TB 870 EVO solid-state drive (Samsung Electronics Co., Ltd., Suwon, Gyeonggi-do, Republic of Korea).

Software environment

The robot software system was built on the Ubuntu 20.04 operating system (https://ubuntu.com/) using Robot Operating System (ROS) Noetic (https://www.ros.org/) as the development framework. The deep learning module used PyTorch 1.18 (https://pytorch.org/) combining with TensorRT 8.4 (https://developer.nvidia.com/tensorrt) for model inference acceleration. The path planning algorithm was implemented in Python 3.8 (https://www.python.org/) and relied on OpenCV 4.5 (https://opencv.org/) for image preprocessing. The core control program was written in C++, and each functional module communicated and interacted *via* ROS topics and services. The system integrated Matplotlib (https://matplotlib.org/), RViz (a built-in visualization tool of ROS), and Open3D (http://www.open3d.org/) for multidimensional data visualization and utilized TensorBoard (https://www.tensorflow.org/tensorboard) to realize visual monitoring of model training and testing processes. The simulation scene was built based on Unity 3D 2022.3 (https://unity.com/). Classic algorithms included the traditional A* algorithm, Dijkstra algorithm, Rapidly-exploring Random Tree Star (RRT*) algorithm, U-Net, Faster R-CNN, and Mask R-CNN. Their implementations in this study were based on open-source code from the PyTorch ecosystem, and all open-source repositories were publicly available on GitHub (https://github.com/).

Experimental dataset

The experimental dataset for corn diseases covered samples of six common diseases including large spot disease, small spot disease, rust disease, curvaceous fungus leaf spot disease, gray spot disease, and sheath blight, as well as healthy leaf samples. The data was collected from the corn planting base in Xinxiang, Henan, China, covering different growth stages and environmental conditions. A total of 15,000 samples were collected and divided into training set of 12,000, validation set of 1,500, and test set of 1,500. Each sample contained RGB images, infrared images, synchronized environmental data, and complete disease labeling information.

Experimental scene setting

The experimental scenes were divided into two categories of simulation and field. The simulation scene was built based on Unity 3D, setting up a virtual corn field of 100 meters square, covering various ridge spacing, obstacle density, and environmental complexity configurations for module performance testing and algorithm optimization. The on-site scene was in a large-scale corn planting base in Xinxiang, Henan, China. Three different areas of fields were selected including various terrain conditions and disease distribution patterns, mainly for robot overall performance testing and system application verification.

Path planning algorithm comparison

To verify the superiority of the improved A* algorithm, this study selected traditional A* algorithm, Dijkstra algorithm, and Rapidly-exploring Random Tree Star (RRT*) algorithm as comparison methods and conducted tests in a simulated corn field environment. The simulation environment was set to 100 m × 100 m with a ridge spacing of 0.8 m and five fixed obstacles. The test results were statistically analyzed based on four indicators including path length, planning time, number of turns, and path confidence.

Detection-segmentation-grading module performance evaluation

To evaluate the performance of the proposed detection-segmentation-grading integrated module, this study used the test set for comprehensive validation and selected YOLOv8 combined with U-Net and Faster R-CNN combined with Mask R-CNN as comparison models. The performance evaluation mainly focused on four indicators of detection accuracy, segmentation accuracy, grading accuracy, and inference speed.

Multi-sensor fusion perception performance comparison experiment

To verify the superiority of the multi-sensor dynamic weighted fusion module, this study selected fixed-weight fusion and single visual perception schemes as controls. In the fixed-weight fusion scheme, the visual weight was set to 0.5, the positioning data weight was 0.2, the ultrasound weight was 0.2, and the environmental sensor weight was 0.1. The performance of each test scheme in terms of perception accuracy, data transmission delay, and system credibility under different environmental complexities was tested and compared.

Extreme environment adaptability test

To verify the adaptability of the framework in extreme environments, three extreme scenarios were selected including high temperature (38℃), rainy weather, and severe occlusion to test the overall performance of the framework with the conventional environment as the control group.

Statistical analysis

All experimental data were statistically analyzed using SPSS 26.0 statistical software (IBM, Armonk, NY, USA). One-way analysis of variance (ANOVA) was used to compare the performance differences among multiple algorithms / models / schemes, and the least significant difference (LSD) method was used for post-hoc pairwise comparison. *P* value less than 0.05 was considered statistically significant. All quantitative data were presented as mean ± standard deviation, and each group of experiments was repeated 5 times independently to ensure the reliability of the results.

Results and discussion

Performance testing of improved A* path planning algorithm

The results demonstrated that the improved A* algorithm proposed in this study performed well in multiple performance indicators. Compared with the traditional A* algorithm, the path length was shortened by 4.8%, while compared with Dijkstra and RRT* algorithms, it was shortened by 9.7% and 15.2%, respectively, significantly reducing redundancy. The algorithm planning time was only 32.4 milliseconds, which was 29.1% less than the traditional A* algorithm and had good real-time performance. In addition, the number of path turns had been significantly reduced by 46.7%, and the smoothness of the path had been significantly optimized. In terms of path confidence, this algorithm achieved 0.93, which was higher than other compared algorithms, demonstrating stronger path rationality and environmental adaptability. It increased the average running speed of the robot to 1.10 meters per second and significantly improved inspection efficiency (Table 1). To further verify the adaptability of the improved A* algorithm under different ridge spacing, the ridge spacing was set to 0.6, 0.8, and 1.0 m in the simulated scene. The path adjustment time and offset error of the algorithm were tested. The results showed that, as the ridge spacing increased from 0.6 to 1.0 m, the path adjustment time gradually increased from 28.7 to 35.2 ms with an overall change of only 22.6%, indicating that the algorithm had a fast response ability to changes in ridge spacing. Meanwhile, the path deviation error was always controlled within 5 cm, and the error reached its minimum of 2.3 cm at 0.8 m ridge spacing. At 0.6 m and 1.0 m ridge spacings, the errors were 3.8 cm and 4.5 cm, respectively, which met the actual requirements of inter ridge operations. Compared with the traditional A* algorithm, which generally had an offset error of 8 to 12 cm, the proposed algorithm significantly improved the adaptability of ridge spacing (Figure 1).

Performance testing of integrated detection segmentation grading module

The detection accuracy of the proposed model reached 95.6%, which was 6.3 percentage points higher than the YOLOv8 and U-Net combined model, and 5.5 percentage points higher than the Faster R-CNN and Mask R-CNN combined model. In the segmentation task, the IoU of the model

Table 1. Performance comparison of different path planning algorithms.

Algorithm	Path length (m)	Planning time (ms)	Number of turns (turn)	Path confidence level	Average speed (m/s)
Dijkstra's	142.6	89.3	18	0.78	0.85
Traditional A*	135.2	45.7	15	0.85	0.92
RRT * algorithm	151.8	102.5	22	0.72	0.78
Improved A*	128.7	32.4	8	0.93	1.10

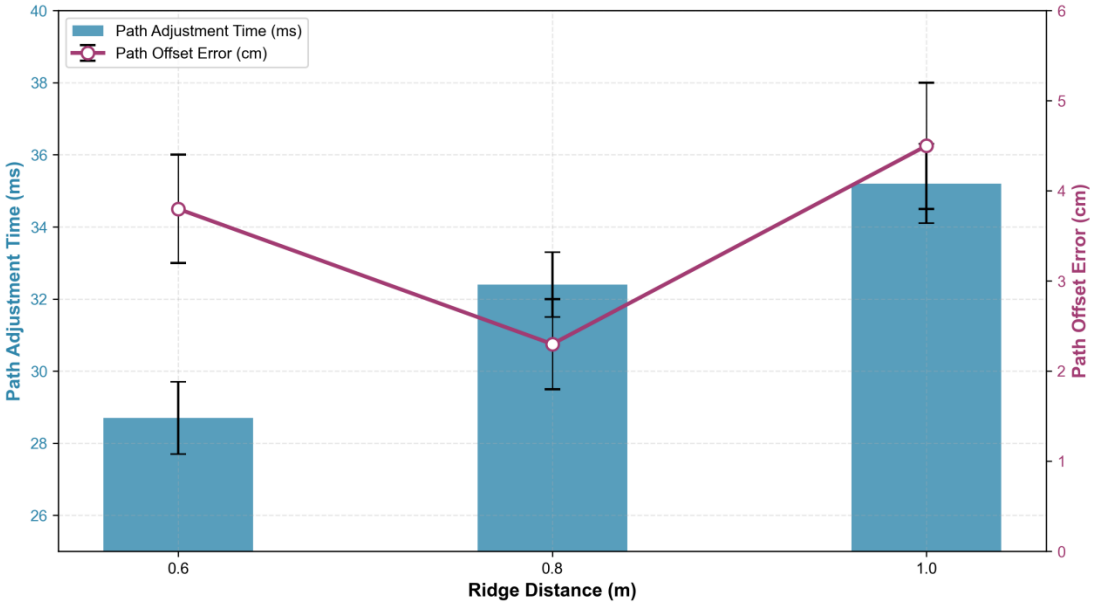


Figure 1. Adaptability test of improved A* algorithm under different ridge spacing.

reached 89.2%, which was 6.7 and 5.5 percentage points higher than the comparison model, respectively. The grading accuracy was outstanding, reaching 93.7%, significantly higher than the accuracy of conventional grading models, which was 85.3%. In terms of inference speed, this model achieved a processing capacity of 35 frames per second, which was 7 frames and 20 frames higher than the two compared models, respectively (Table 2). The performance improvement was mainly due to the integrated structure design of detection segmentation grading, optimization of joint loss function, and effective integration of attention mechanism, which significantly improved computational efficiency while maintaining high accuracy, fully meeting the needs of real-time robot inspection.

To visually demonstrate the segmentation effect, four typical disease samples were selected for comparison of segmentation results with each displaying the original RGB image, infrared fusion image, traditional model segmentation results, and the segmentation results of proposed model. The first group consisted of large spot disease samples with brown elongated lesions visible in the original image. Infrared fusion enhanced the contrast of the lesions, while traditional models suffered from edge blurs and background residue. The proposed model achieved accurate segmentation with an edge integrity of over 95%. The second group consisted of rust samples, and the original image leaves were covered with small yellow spots. Traditional models had missed the detection of small spots, but

Table 2. Performance comparison of different detection, segmentation, and grading models.

Model	Detection accuracy (mAP@0.5) (%)	Segmentation accuracy (IoU) (%)	Grading accuracy (%)	Inference speed (FPS)
YOLOv8 + U-Net (without grading branch)	89.3	82.5	-	28
Faster R-CNN + Mask R-CNN (without grading branch)	90.1	83.7	-	15
YOLOv8 + U-Net + Simple Grading	91.5	84.2	85.3	25
Proposed model (improved YOLOv8 + U-Net++ + grading branch)	95.6	89.2	93.7	35

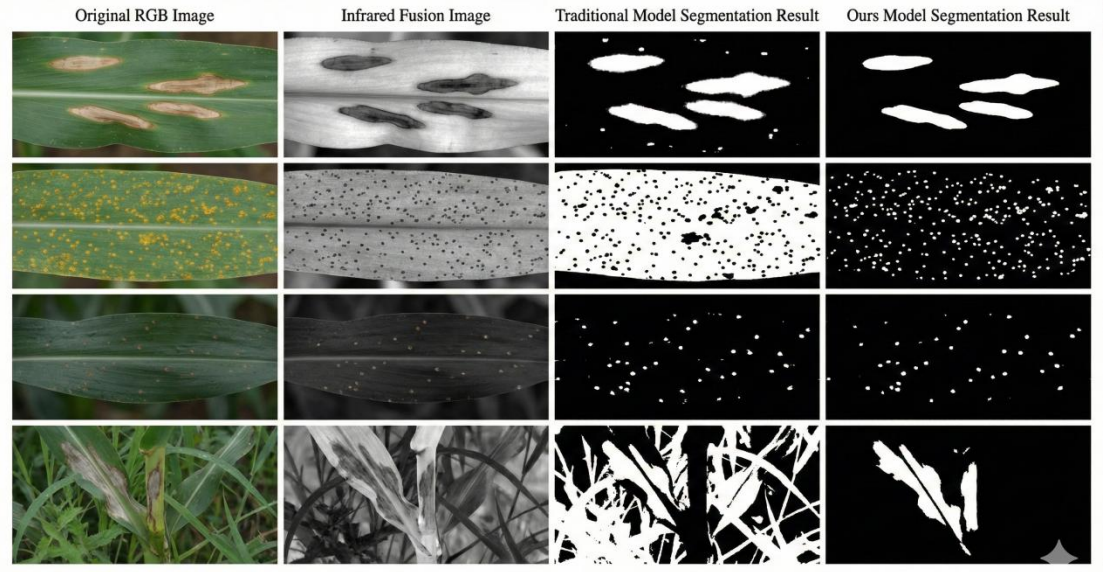


Figure 2. Comparison of physical images of corn disease segmentation effects.

proposed model reduced the missed detection rate to below 2% through attention mechanism. The third group consisted of small spot disease samples in rainy and overcast environments, where the original images had insufficient lighting and low contrast, resulting in a decrease in traditional model segmentation accuracy. The proposed model combined infrared fusion and environmental adaptive enhancement, while maintaining high segmentation integrity. The fourth group consisted of samples of sheath blight in occluded environments. Traditional models mistakenly identified the parts of leaves obscured by weeds as disease spots. The proposed model effectively eliminated occlusion interference through bounding box prior constraints and semantic segmentation optimization, achieving a segmentation IoU of 0.88 (Figure 2). To verify the performance of the grading module, the grading accuracy of different types of diseases was calculated and showed that the average grading accuracy of the grading module for 6 types of corn diseases was 93.5% with the highest grading accuracy for severe diseases as 94.4% and relatively low grading accuracy for mild diseases as 92.1%, which might be because mild diseases had small lesion areas and unclear characteristics that were easily confused with natural aging spots on leaves. Specifically, the average grading accuracies of

Table 3. Comparison of grading accuracy for different disease types.

Disease type	Mild accuracy rate (%)	Moderate accuracy (%)	Severe accuracy rate (%)	Average grading accuracy (%)
Large spot disease	92.3	95.6	94.1	94.0
Small spot disease	93.7	94.8	92.9	93.8
Rust	91.5	92.6	95.3	93.1
Curvularia leaf spot	90.8	93.4	94.7	93.0
Gray spot disease	92.1	93.9	94.5	93.5
Sheath blight	91.9	94.2	95.1	93.7
Average	92.1	94.1	94.4	93.5

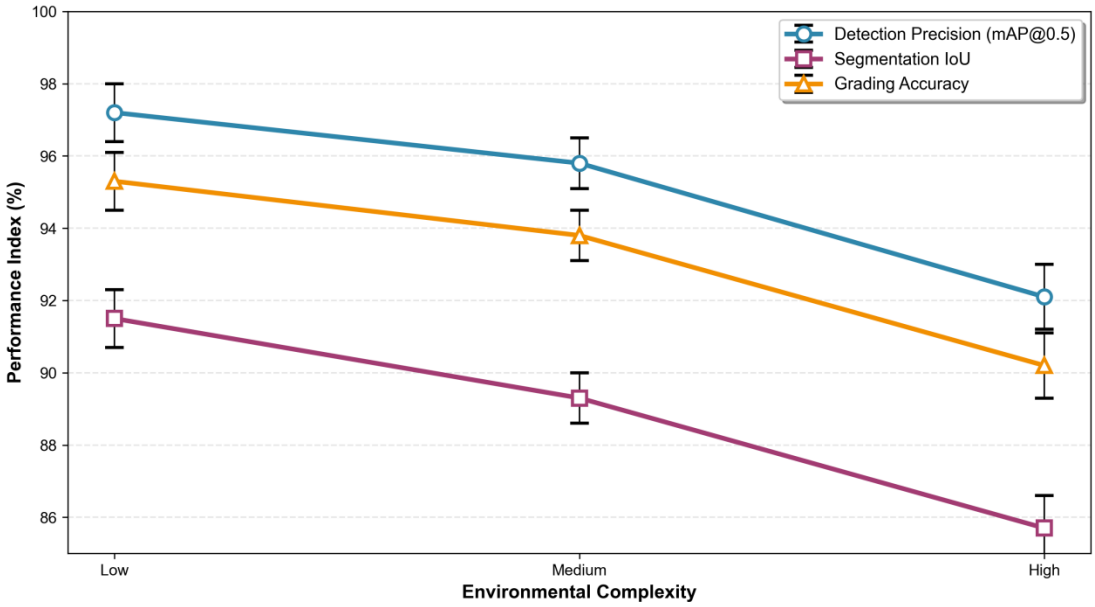


Figure 3. Performance test for the integrated module under varying levels of environmental complexity.

large spot disease, small spot disease, and sheath blight all exceeded 93.7%, showing the best performance. The average grading accuracy of *Curvularia* leaf spot disease was 93.0% (Table 3), slightly lower than the overall level, mainly due to the diverse morphology and irregular edges of the disease spots, making it difficult to adapt the grading threshold. Overall, the grading module could accurately match the severity characteristics of different diseases. Combined with the dynamic adjustment of environmental impact factors, it could effectively support subsequent precise prevention and control decisions. To verify the robustness of the integrated module under different environmental complexities, low, medium, and high environmental complexities were set in the simulated scenario to test the detection accuracy, segmentation IoU, and grading accuracy of the module. The results demonstrated that, at low environmental complexity, the detection accuracy reached 97.2%, the segmentation IoU was 91.5%, and the grading accuracy was 95.3%. When the environmental complexity was moderate, the three indicators were 95.8%, 89.3%, and 93.8%,

Table 4. Performance comparison of different environmental perception schemes.

Perception scheme	Environmental complexity	Perception accuracy (%)	Data transmission delay (ms)	Fusion credibility
Single visual perception	Low	96.3	18.5	0.92
	Medium	88.7	19.2	0.83
	High	75.2	20.1	0.68
Fixed-weight fusion	Low	96.8	25.3	0.93
	Medium	90.5	26.7	0.85
	High	80.3	27.5	0.73
Proposed dynamic weighted fusion	Low	97.5	28.6	0.95
	Medium	94.7	29.8	0.90
	High	88.9	31.2	0.82

Note: In the fixed-weight fusion scheme, the weights of vision, positioning, ultrasound, and environmental sensors were set to 0.5, 0.2, 0.2, and 0.1, respectively.

respectively, with a decrease of less than 1.5 percentage points. Under high environmental complexity conditions, the detection accuracy, segmentation IoU, and grading accuracy were 92.1%, 85.7%, and 90.2%, respectively. Although there was a slight decrease, they were still significantly higher than the highest performance of the comparison model at 88%, 80%, and 85% (Figure 3). The result indicated that the proposed module could effectively resist the interference of complex environments through infrared image fusion, attention mechanism, and environment adaptive enhancement. Its robustness met the practical needs of corn field inspection.

Performance testing of multi-sensor fusion environment perception module

The performance of various testing schemes in terms of perception accuracy, data transmission delay, and system credibility under different environmental complexities showed that the dynamic weighted fusion module performed the best in different environmental complexities with 97.5% perception accuracy at low environmental complexities, which was 1.2 percentage points higher than single visual perception and 0.7 percentage points higher than fixed weight fusion. The fusion credibility reached 0.95, and the data transmission delay was 28.6 ms, meeting real-time requirements. Under moderate environmental complexity, the perception accuracy was 94.7%, which was 6.0 percentage points and 4.2 percentage points higher than the comparison scheme, respectively. The fusion credibility remained above 0.90. Under high environmental complexity, the perception accuracy still reached 88.9%, which was 13.7 percentage points higher than single visual perception and 8.6 percentage points higher than fixed weight fusion. The fusion credibility was 0.82, significantly higher than the comparison scheme, indicating that the dynamic weight allocation mechanism could adaptively adjust the weights of each sensor according to environmental changes, effectively improving the perception reliability in complex environments. Although the data transmission delay was higher than the comparison scheme, the maximum delay was only 31.2 ms, which did not affect the real-time response of robot inspection (Table 4). To visually demonstrate the improvement effect of multi-sensor fusion on disease detection, the study selected corn rust samples from rainy and obstructed scenes under high environmental complexity conditions and compared and analyzed the detection and segmentation effects of three perception schemes. The results demonstrated the

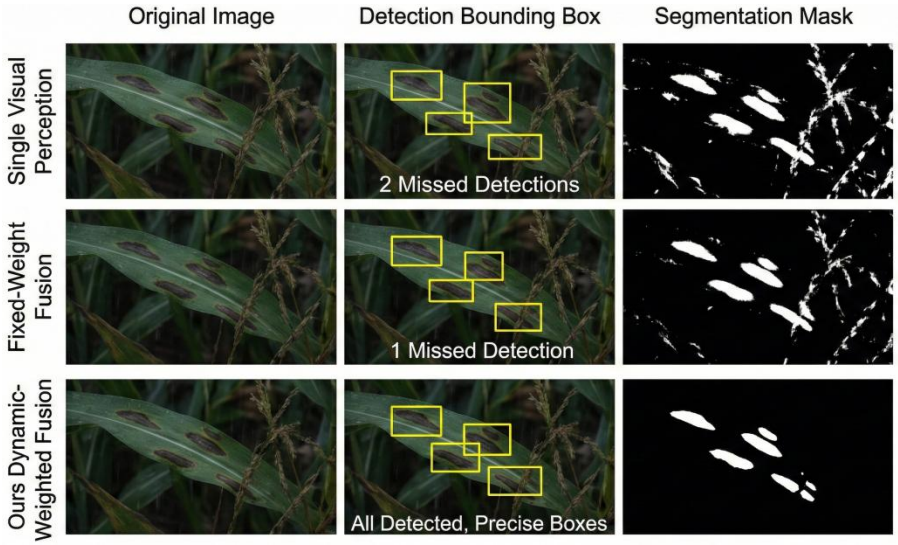


Figure 4. Comparison of segmentation effects detected by different perception schemes.

detection and segmentation results of dynamic weighted fusion including the original image, detection box annotation, and segmentation mask for each group of images. The single visual perception scheme was affected by insufficient rainy and cloudy lighting and weed obstruction, resulting in 2 missed disease spots and obvious background residue in the segmentation mask. The detection confidence was only 0.72. The fixed weight fusion scheme reduced one missed detection, but the segmentation edges were still blurry with a detection confidence of 0.81. The dynamic weighted fusion scheme in this article accurately detected all lesions through deep fusion of infrared images and visual images with clear segmentation mask edges, no background residue or misclassification, and a detection confidence of 0.94, fully demonstrating the advantages of the dynamic weighted fusion mechanism in complex environments (Figure 4).

Overall framework performance testing

The results showed that the proposed framework significantly outperformed the comparative framework in both simulated and real-world scenarios. In the simulated scenario, the success rate of target search reached 98.2%, an increase of 9.7 percentage points compared to the comparative framework. The inspection omission rate was only 2.1%, a decrease of 6.6 percentage points compared to the comparative framework. The path planning took 32.7 ms, which was 13.5 ms shorter than the comparative framework. The inspection efficiency reached 5,240 m²/h, which was 35.8% higher than the comparative framework. In the field scenario, as the field area increased, the advantages of the proposed framework became more apparent. In the 300 m × 300 m field scenario, the success rate of target search was 95.7%, which was 13.0 percentage points higher than the comparative framework. The inspection omission rate was controlled within 4.2%, which was 8.3 percentage points lower than the comparative framework. The path planning time remained stable at 34.5 ms, which was 16.8 ms lower than the comparative framework, highlighting the real-time advantage. The inspection efficiency reached 11,600 m²/h, which was 33.3% higher than the comparative framework and could meet the rapid inspection needs of large-scale corn fields (Table 5). The adaptability of the framework in extreme environments demonstrated that the proposed framework exhibited high performance stability in extreme environments such as high temperature, rainy weather, and severe occlusion. The framework had a success rate of over 91.5% in target search, a missed inspection

Table 5. Overall performance comparison of the framework.

Test scenario	Frame type	Target search success rate (%)	Inspection omission rate (%)	Path planning time (ms)	Inspection efficiency (m^2/h)
Simulated scene (100 m × 100 m)	Conventional Agricultural Inspection Robot Framework	88.5	8.7	46.2	3860
Simulated scene (100 m × 100 m)	Proposed framework	98.2	2.1	32.7	5240
Field scene (50 m × 50 m)	Conventional Agricultural Inspection Robot Framework	85.3	10.2	48.5	920
Field scene (50 m × 50 m)	Proposed framework	96.8	3.5	33.1	1280
Field scene (300 m × 300 m)	Conventional Agricultural Inspection Robot Framework	82.7	12.5	51.3	8700
Field scene (300 m × 300 m)	Proposed framework	95.7	4.2	34.5	11600

Note: The conventional agricultural inspection robot framework integrated the traditional A* algorithm, YOLOv8 detection model, and fixed-weight sensor fusion.

Table 6. Overall performance testing of the framework under extreme environments.

Extreme environmental types	Target search success rate (%)	Inspection omission rate (%)	Detection accuracy (%)	Stability of path planning (%)
High temperature (38℃)	94.3	4.8	89.7	96.5
Rainy and overcast weather	92.8	5.5	87.2	95.8
Heavy occlusion	91.5	6.1	85.3	94.2
Conventional environment (control)	97.3	3.1	95.9	98.7

rate controlled within 6.1%, a detection accuracy rate of over 85%, and a path planning stability of over 94.2%. Compared with the conventional environment, although all indicators had slightly decreased, the decrease had not exceeded 6 percentage points, which was significantly better than the existing inspection system that the latter's detection accuracy in extreme environments was usually lower than 75%, and the missed detection rate was higher than 15% (Table 6). The results indicated that the proposed framework effectively enhanced the system's ability to resist extreme environmental interference by adopting multi-sensor dynamic weighted fusion, environment adaptive enhancement, and improved path planning algorithms, thus better adapting to the complex and changing practical inspection needs of corn fields.

Conclusion

This study proposed a fast target-search framework for corn disease inspection robots. The constructed four-level topology framework of perception-decision-execution-evaluation integrated three core functional modules, realizing efficient processing of the whole process of corn disease inspection. The framework had a reasonable structure and good environmental adaptability, which could effectively cope with the complex and changing practical inspection demands of corn fields. The

improved A* path planning algorithm that incorporated micromouse wall distance perception and fast turning logic with an additional ridge distance adaptive mechanism could effectively improve the efficiency and adaptability of inter-ridge inspection in corn fields. The integrated detection-segmentation-grading module could accurately extract disease category, location, area, and severity information, providing data support for precise prevention and control decisions. The multi-sensor dynamic weighted fusion module that adaptively adjusted weights according to environmental complexity significantly improved the adaptability and robustness of the framework to complex environments. Deployed on the inspection robot, the proposed framework showed excellent overall performance in field scenarios, providing an efficient and reliable technical solution for rapid disease inspection in large-scale corn fields, and was suitable for the upgrading of modern agricultural intelligent equipment scenarios. Future research should focus on optimizing the path planning algorithm to improve its dynamic adaptability in complex terrain and dense obstacle environments by integrating reinforcement learning and deep learning, promoting the lightweight design of detection and grading modules, using model quantization and pruning techniques to reduce deployment costs and support large-scale application promotion, further expanding system functions, combining Internet of Things technology to realize real-time transmission and cloud analysis of inspection data, and building an intelligent operation system covering the whole process of inspection, evaluation, and prevention and control, so as to provide more comprehensive technical support for precision crop protection in modern agriculture.

Acknowledgement

This study was funded by Henan Province's Science and Technology Research Project (Grant No. 262102221041).

References

1. Wong WK, Ye S, Liu H, Li Y, Zhang Q, Chen L, *et al*. 2022. Effective mobile target searching using robots. Mob Netw Appl. 27(1):249-265.
2. Liu Y, Shu X, Sun Y, Wang H, Zhang Z, Li M, *et al*. 2022. RAPID: real-time alert investigation with context-aware prioritization for efficient threat discovery. Proc 38th Annu Comput Secur Appl Conf. 38:827-840.
3. Luo Q, Luan TH, Shi W, Li C, Wang X, Yang F, *et al*. 2022. Deep reinforcement learning based computation offloading and trajectory planning for multi-UAV cooperative target search. IEEE J Sel Areas Commun. 41(2):504-520.
4. Garritty C, Hamel C, Trivella M, McKenzie JE, Ryan R, Brennan SE, *et al*. 2024. Updated recommendations for the Cochrane rapid review methods guidance for rapid reviews of effectiveness. BMJ. 384:e077621.
5. Liao V, Myers T, Jayaraman A. 2024. A computational method for rapid analysis polymer structure and inverse design strategy (RAPSIDY). Soft Matter. 20(41):8246-8259.
6. Merry L, Castiglione SA, Rouleau G, Dhollander T, De Paepe N, Van den Bussche K, *et al*. 2023. Continuing professional development (CPD) system development, implementation, evaluation and sustainability for healthcare professionals in low-and lower-middle-income countries: A rapid scoping review. BMC Med Educ. 23(1):498.
7. Panagoulias DP, Virvou M, Tsihrintzis GA. 2024. A novel framework for artificial intelligence explainability *via* the technology acceptance model and rapid estimate of adult literacy in medicine using machine learning. Expert Syst Appl. 248:123375.
8. Okabaka IE, Olwenyi E, Naikoba S, Onyango OA, Wanjala R. 2023. Design and development of a robot for monitoring common rust, blight and gray leaf spot diseases in maize. J Agric Eng. 54(3):12-21.
9. Moshayedi AJ, Khan AS, Geng K, Li J, Wang Y, Chen L, *et al*. 2025. Advancing agricultural practices: Analyzing the role of robotics in corn farming. Int J Eng Trans A Basics. 38:1517-1532.
10. Stypulkowska J. 2023. The use of AI to determine the condition of corn in a field robot that meets the requirements of precision farming. FedCSIS Commun Pap. 10:215-222.
11. Li X, Chen Z, Uppuluri RS, Zhang Y, Wang L, Tang H, *et al*. 2025. Robotic system with tactile-enabled leaf tracking for high-resolution hyperspectral imaging device for autonomous corn leaf phenotyping in controlled environments. Smart Agric Technol. 7:101427.
12. Pfordt A, Paulus S. 2025. A review on detection and differentiation of maize diseases and pests by imaging sensors. J Plant Dis Prot. 132(1):40.
13. Zhang XW, Yi KC. 2023. Research on motion planning model and control strategy of corn inspection robot. J Agric Mech Res. 45(11):189-194.
14. Diao Z, Ma S, Li J, Wang H, Zhang Y, Liu X, *et al*. 2025. Navigation line detection algorithm for corn spraying robot based on improved LT-YOLOv10s. Precis Agric. 26(3):1-23.
15. Tomas MCA, Gonzales MAC, Pasia JCG, Reyes JLD, Cruz ED. 2024. Detection of corn leaf diseases using image processing

and YOLOv7 convolutional neural network (CNN). Proc 9th Int Conf Intell Inf Technol. 9:134-140.
16. Wang H, Lou S, Jing J, Li Y, Zhang H, Liu Z. 2022. The EBS-A* algorithm: An improved A* algorithm for path planning. PLoS One. 17(2):e0263841.
17. Orozco-Rosas U, Picos K, Pantrigo JJ, Montemayor AS, Piña J. 2022. Mobile robot path planning using a QAPF learning algorithm for known and unknown environments. IEEE Access. 10:84648-84663.
18. Ait Saadi A, Soukane A, Meraihi Y, Benmessaoud Gabis A, Mirjalili S, Ramdane-Cherif A. 2022. UAV path planning using optimization approaches: A survey. Arch Comput Methods Eng. 29(6):4233-4284.
19. Zhang W, Wang N, Wu W. 2023. A hybrid path planning algorithm considering AUV dynamic constraints based on improved A* algorithm and APF algorithm. Ocean Eng. 285:115333.
20. Suresh KS, Venkatesan R, Venugopal S. 2022. Mobile robot path planning using multi-objective genetic algorithm in industrial automation. Soft Comput. 26(15):7519-7531.
21. Chen N, Feng Z, Li F, Wang H, Zhang L, Zhao Y. 2023. A fully automatic target detection and quantification strategy based on object detection convolutional neural network YOLOv3 for one-step X-ray image grading. Anal Methods. 15(2):164-170.
22. Dinesh P, Lakshmanan R. 2025. Multiclass semantic segmentation for prime disease detection with severity level identification in Citrus plant leaves. Sci Rep. 15(1):21208.
23. Fang S, Zhang B, Hu J. 2023. Improved mask R-CNN multi-target detection and segmentation for autonomous driving in complex scenes. Sensors. 23(8):3853.
24. Mzoughi O, Yahiaoui I. 2023. Deep learning-based segmentation for disease identification. Ecol Inform. 75:102000.
25. Kousar S, Afzal M, Ahmed F, Naseer K, Shaheen S, Bibi S, *et al*. 2022. Environmental awareness and air quality: The mediating role of environmental protective behaviors. Sustainability. 14(6):3138.
26. Tabuenca B, Moreno-Sancho JL, Arquero-Gallego J, Rodriguez-Sanchez MC. 2023. Generating an environmental awareness system for learning using IoT technology. Internet Things. 22:100756.
27. Saehu MS, Diah AM, Julca-Guerrero F, Arifin M. 2022. Environmental awareness and environmental management practices: Mediating effect of environmental data distribution. J Environ Manag Tour. 13(5):1339-1352.
28. Feng X, Zhang Z, Chen Q, Guo Z, Zhang H, Wang M, *et al*. 2025. Integrating remote sensing, GIS, and multi-criteria decision making for assessing PV potential in mountainous regions. Renewable Energy. 241:122340.
29. Li L, Lu Y, Wang Y, Zheng Q, Li W. 2025. Mxplainer: Explain and learn insights by imitating mahjong agents. Algorithms. 18(12):738.